Journal of Materials Chemistry

Dynamic Article Links

Cite this: J. Mater. Chem., 2012, 22, 7050

www.rsc.org/materials

PAPER

Dramatic enhancements in toughness of polyimide nanocomposite *via* long-CNT-induced long-range creep†

Xilai Jia,[a] Qiang Zhang,*[a] Meng-Qiang Zhao,[a] Guang-Hui Xu,[a] Jia-Qi Huang,[a] Weizhong Qian,[a] Yunfeng Lu*[b] and Fei Wei*[ac]

Received 21st October 2011, Accepted 9th February 2012
DOI: 10.1039/c2jm15359a

Super tough carbon nanotube (CNT) reinforced nanocomposites require both the unique interaction and effective stress transfer between CNTs and polymer chains. When CNT reinforced nanocomposites are stretched, the crack interfaces are usually bridged by CNTs, and energy can be absorbed during deformation before fracture and bring high toughness. However, developing super-tough CNT/polymer nanocomposites which can withstand high matrix deformation yet exploit the superior strength of CNTs is still a great challenge. In this contribution, an ultra-tough CNT/polyimide (PI) nanocomposite was fabricated by a facile *in situ* polymerization. Super-long vertically aligned CNTs were dispersed into *N*,*N*-dimethylacetamide, which is the feedstock for *in situ* PI polymerization. A long-CNT-induced three-dimensional, continuous, and heterogeneous network is formed to toughen the nanocomposites. By incorporating 0.27 wt% CNTs into a PI matrix, the tensile strength and elongation at break of the nanocomposites reached 156.4 MPa and 140%, respectively, which are 90% and 250% increased compared with the values of pristine PI. Thus, the toughness of the nanocomposites improved 470% and approached 127.4 J g^{-1}, well exceeding state-of-the-art tough materials. The reinforcement mechanism reveals that robust tapered fibrils are formed around high-aspect-ratio CNTs to facilitate energy dissipation and enhance the energy absorbing capability. The length of CNTs and the interfacial bonding are important to initiate long-range creep and form robust heterogeneous tapered fibrils to toughen the nanocomposites. The CNT/PI composite film with high toughness, much improved electrical conductivity, as well as high thermal stability, and transparency, broadened their advanced applications in aerospace, aviation, buildings, bulletproof vests, and so on.

1. Introduction

Toughness is the ability of a material to absorb energy during deformation before fracture. High toughness materials find a spectrum of important applications such as aerospace, airplanes, buildings, and bulletproof vests.[1] Traditional composite materials, such as glass fiber and carbon fiber reinforced composites, are often strong but not tough. Therefore, exploring new tough materials is in high demand. Carbon nanotubes (CNTs) are one of the strongest known materials, with 50–100 GPa strength and more than 1 TPa modulus. Due to their unique mechanical properties, they have been ubiquitous in exploiting high performance nanocomposites.[2,3]

Transferring the unique mechanical properties of individual CNTs into a macroscopic composite is a great challenge. Extensive research on improving mechanical properties of CNT/polymer nanocomposites has been carried out over the past years, especially on the improvement of tensile strength and modulus.[4–6] The toughening of CNT/polymer composites, however, remains poorly understood despite widespread studies. The common toughening mechanism of CNT-based nanocomposites is that crack interfaces are bridged by CNTs. As illustrated in Scheme 1a, when the interaction between CNTs and polymer matrix is weak, CNTs are easily interfacial debonding, and pulled out of the matrix; thus, limited improvement of toughness is shown. In another case, strong bonding between CNTs and polymer matrix results in CNT breakdown (Scheme 1b). Even though the addition of CNTs increases the yield strength and modulus of such composites, the toughness of the composite is still not satisfactory when polymers are brittle. Thus, developing CNT/polymer composites which can withstand

[a]*Beijing Key Laboratory of Green Chemical Reaction Engineering and Technology, Department of Chemical Engineering, Tsinghua University, Beijing 100084, P. R. China. E-mail: zhang-qiang@mails.tsinghua.edu.cn; wf-dce@tsinghua.edu.cn; Fax: +86-10-6277-2051; Tel: +86-10-6278-5464*

[b]*Departments of Chemical Engineering and Materials Science Engineering, University of California, Los Angeles, California, 90095, USA. E-mail: luucla@ucla.edu*

[c]*Center for Nano and Micro Mechanics, Tsinghua University, Beijing 100084, P. R. China*

† Electronic supplementary information (ESI) available. See DOI: 10.1039/c2jm15359a

high matrix deformation yet exploit the superior strength of CNTs is necessary.

Agglomerated CNTs, in which CNTs are entangled with each other, have been mass produced[7] and widely used as raw materials for nanocomposite fabrication.[2,5] The first step is to disperse them in solution by ultrasonication with a surfactant, acid assisted high temperature cutting, and ball milling.[8] During these treatments, CNTs were cut to less than 1 μm.[8] The as-obtained composites consisted of analogues of random short CNTs. Some trials have been employed to get CNT nanocomposites from super-long aligned CNTs, however, the lengths of CNTs are still cut down to *ca.* 1 μm if sonication is employed.[9] The pre-dispersion of CNTs and post-mixing with the polymer matrix cause a lot of difficulty for uniform distribution of long CNTs (more than 20 μm) in nanocomposites. *In situ* polymerization of the polymer matrix from solvent in which super-long CNTs are well dispersed is a combined route for CNT dispersion and nanocomposite fabrication. In the as-obtained nanocomposites, interactions between polymer chains and CNTs match well, leading to the mobility of macromolecule chains during the stretching process (Scheme 1c). Thus, a super-tough nanocomposite film is highly expected. Selecting the proper polymer matrix and related processing for the nanocomposite is a key issue.

Herein, we explore the idea of fabrication of ultra-tough polyimide (PI) nanocomposites containing high-aspect-ratio CNTs using *in situ* polymerization. Aromatic PI is selected as the matrix because of its good tensile strength, excellent flexibility, and strong non-covalent 'π–π' interactions with CNTs.[6,10] Various combinations of PI with CNT fillers, including pristine CNTs, purified CNTs, acid oxidized CNTs and functionalized CNTs, have been extensively reported.[6,11,12] For instance, Jung *et al.* proposed a novel route to the fabrication of strong and transparent CNT/PI films reinforced with individually dispersed double-walled CNTs based on the introduction of chemical moieties of the outer tubes combined with an *in situ* polymerization.[6] However, to the best of our knowledge, CNTs in PI or other polymer matrices are always short (less than 5 μm for individual CNTs) because of the processing applied and the inherent limitation of the obtained CNTs. Herein, long CNTs, as well as trapped PI macromolecules in the matrix form a network for effective load transfer. As illustrated in Scheme 1c, robust fibrils in the CNT/PI composite form. The fibrils show a tapered structure, where PI macromolecules tightly orient CNTs and become stiffened under tension. The fibrils utilize CNT strength and PI deformation capability to produce tough nanocomposites. Even with a low nanotube content, the toughness of the as-fabricated CNT/PI nanocomposites has been highly improved due to the induced robust fibrils. Multifunctional properties of the composites have been investigated to broaden their advanced functional applications.

2. Experimental section

Materials

Pyromellitic dianhydride (PMDA, analytical reagent (AR) grade) and 4,4-oxydianiline (ODA, AR) were purchased from Shanghai Chemicals Co. (Shanghai, China). *N*,*N*-Dimethylacetamide (DMAc, AR) was purchased from Beijing Chemicals Co. (Beijing, China). Pristine aligned CNTs were purified using an 18% HCl solution and a 20% HF solution alternatively to remove residual catalysts. As control, weakly oxidized CNTs (w-CNTs) were prepared by slight oxidation of purified CNTs with cooled piranha solutions (4 : 1, vol/vol 96% H_2SO_4/30% H_2O_2) at 25 °C for 100 min while strongly oxidized CNTs (s-CNTs) were treated with an oxidative acid mixture (3 : 1 vol/vol 96% H_2SO_4/78% HNO_3) at 110 °C for 100 min in a hydrothermal tank. All CNTs were filtered to pH = 7 and dried in a vacuum oven for 12 h before use.

Fabrication of CNT/PI nanocomposite films

0.25 g of purified aligned CNTs and 300 mL DMAc were placed into an A80 homogenate fluid shearing machine for 1.0 h at a speed of 2000 rpm. Then the solution was centrifuged for 5 min at low speed (about 100 rpm). 20 mL suspension together with 35 mL DMAc was transferred to a three-neck flask under protection of N_2. Next, the suspension was slowly added into 3.0060 g ODA. After stirring for 50 min, 3.3405 g of PMDA was slowly dissolved into the homogeneous mixture. The mixture was stirred at 0 °C for 1.0 h. Extremely viscous PMDA–ODA poly(amic acid) (PAA)–CNT mucus was produced. After degassing with a mechanical vacuum pump, the suspension was cast onto clean glass slides and composite films were formed using a scraper. After 20 h drying under vacuum at 50 °C, PAA films were obtained. The PAA films were then thermally treated in a furnace under Ar at 100, 200, and 300 °C for 30 min, to obtain CNT/PI nanocomposite films. The fabrication of w-CNT/PI and s-CNT/PI composite films was similar to the above mentioned procedure. Fig. 1a describes the schematic illustration of the nanocomposite fabrication and Fig. S1† shows the chemical structure

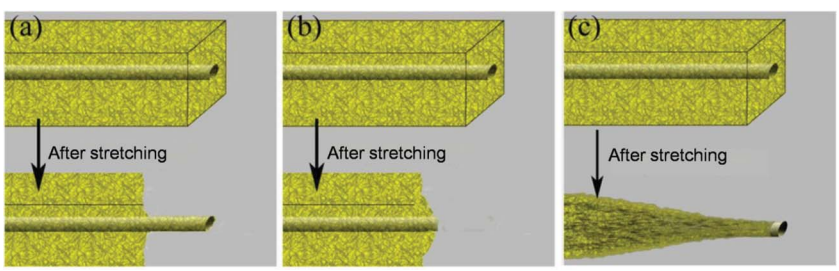

Scheme 1 Fracture models for CNT/polymer composites: (a) pulled out of matrix due to weak interfacial interaction; (b) broken down due to strong interfacial interaction under low deformation; (c) robust fibrils form due to creep from large deformation.

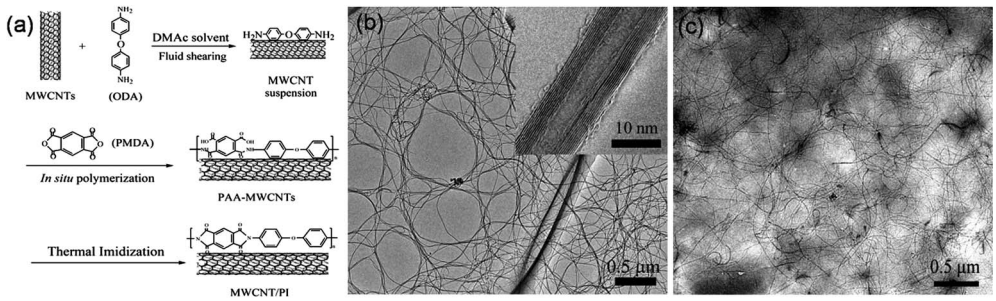

Fig. 1 (a) Schematic illustration for CNT/PI nanocomposite synthesis. (b) TEM image of CNTs after fluid shearing pre-dispersion: due to the large aspect ratio, the CNTs are interwoven into a network; inset is the HRTEM image of an individual CNT. (c) TEM image of CNTs dispersed in the matrix.

of the as-obtained composite films by attenuated total reflection Fourier transform infrared (ATR-FTIR) spectroscopy.

Characterization

FTIR characterization was performed using a Nicolet 6700 spectrometer to identify the effect of purification and oxidization on nanotubes and ATR-FTIR was used to identify the chemical structures of neat PI and CNT/PI films. Optical microscope and transmission electron microscope (TEM, JEOL JEM-2010, 120.0 kV) images were recorded to evaluate the dispersion and distribution of the CNTs in the PI matrix. CNT/PAA gels were transferred to a copper grid and dried under vacuum at 50 °C to prepare the specimen in Fig. 1c. Scanning electron microscopy (SEM) measurements were used to investigate the morphologies of nanotubes and their fracture cross-sections on a JEOL JSM-7401F instrument with an accelerating voltage of 3.0 kV. Thermogravimetric analysis (TGA) was carried out with a thermogravimetric analyzer TGA 2050 instrument from 30–800 °C at a heating rate of 10 °C min^{-1} in air. Volume conductivity was measured on a Keithley 2636A at ambient conditions to evaluate the electrical properties of the composites. UV-vis absorption was measured on an 8453A grating spectrophotometer. Mechanical tests were conducted on a GT-TS-2000 instrument at ambient temperature. The composite films were cut into sheets of 3.0 mm (width) × 10 mm (length) × 65 μm (thickness). They were affixed between two grips. The strips were also weighed with a precise balance to determine the density of samples. The lower grip was fixed and the upper grip rose at a rate of 5.0 mm min^{-1}. Toughness was obtained by integrating the areas under the stress–strain curves and then dividing by the corresponding density around 1380 g cm^{-3}.

3. Results and discussion

3.1 Uniform long CNT distribution in the nanocomposites

As shown in Fig. 1a, CNTs of high aspect ratios are easily dispersed in the precursor mixture of PI. Aromatic PI matrix, together with CNTs, is *in situ* polymerized from PMDA and

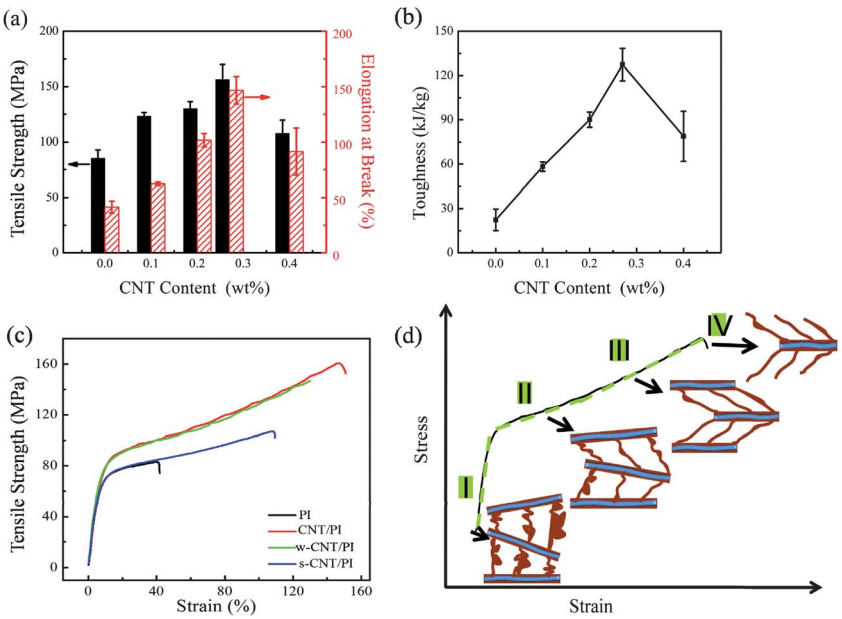

Fig. 2 (a) The tensile strength and elongation at break of long CNT/PI films plotted against their CNT content. (b) Toughness of the as-prepared nanocomposite films. (c) Uniaxial tensile tests of neat PI, CNT/PI, w-CNT/PI, and s-CNT/PI nanocomposites at a constant crosshead speed of 5 mm min^{-1}. (d) Schematic of the obtained self-reinforcement mechanism of CNT/PI nanocomposites.

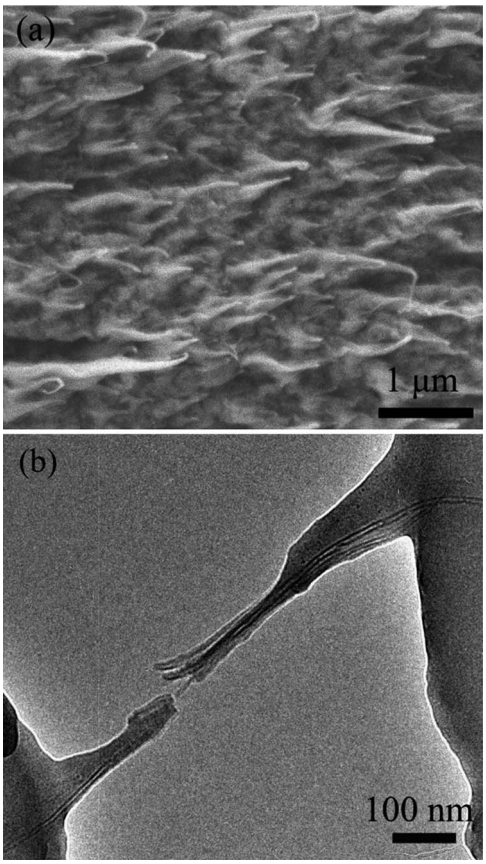

Fig. 3 (a) SEM and (b) TEM images of the typical fracture surface morphology of long CNT/PI composites after ~150% deformation.

ODA. Different from agglomerated CNTs as feedstock, mass-produced aligned CNTs,[13] which were of small diameter (7–15 nm) and long length (~100 μm), were selected as raw CNTs in this contribution. Despite their large aspect ratio, the aligned CNTs are well dispersed with a length distribution of 10–25 μm by fluid shearing in solution,[14] this length distribution is much larger than those achieved by other methods (such as ultrasonication, acid cutting, or ball milling). The TEM image in Fig. 1b shows that the dispersed CNTs are flexible, of high aspect ratio, and easily interwoven into a continuous network. In order to detect the CNT morphology in PI, the precursor mixture was transferred on to a copper gird and dried. The grid was then observed under TEM. Fig. 1c shows TEM micrographs of the CNTs in the matrix. It reveals that CNTs were homogeneously distributed in the nanocomposites and maintained their large aspect ratios, which is essential to enhance the mechanical properties of PI.

3.2 Tough CNT/PI nanocomposites

3.2.1 Effect of CNT content. To fully utilize the high mechanical strength of CNTs and the flexibility of the PI matrix, CNT/PI composites with various compositions were synthesized and characterized. Fig. 2a shows the tensile strength and elongation at break of CNT/PI composites with different CNT loadings. The mechanical properties of as-prepared CNT/PI composites are highly dependent on the CNT content. With increasing amount of CNTs, the tensile strength increases from 82.4 MPa for pure PI to 156.4 MPa for the 0.27 wt% CNT/PI composite. Elongation at break of the nanocomposite film also increases from 40% to 140%, accordingly. In agreement with the optical image (Fig. S2†), the poor dispersion of 0.40 wt% CNTs in PI results in both loss of tensile strength and reduction in elongation at break. The toughness of the nanocomposites is shown in Fig. 2b. The toughness of neat PI is *ca.* 22.4 kJ kg^{-1}. After incorporating 0.27 wt% CNTs, the toughness of the composite dramatically increases up to 127.4 kJ kg^{-1}, corresponding to a 4.7-times improvement (Table 1). The composite toughness (127.4 kJ kg^{-1}) exceeds that of state-of-the-art tough materials, like steel (12 kJ kg^{-1}), Kevlar (33 kJ kg^{-1}), nylon (60 kJ kg^{-1}), rubber (80 kJ kg^{-1}) and other reported tough composite materials (Table S1†).[15] Given the widespread use of PI, the nearly five-fold improvement in toughness reported here is expected to have significant practical applications.

Fig. 2c shows the typical relationship between tensile strength and strain of CNT/PI composites. When the ratio of CNTs incorporated into the film is 0.27 wt%, the composites exhibit the highest tensile stress up to 156 MPa at the highest strain of 150%. The nanocomposite film displays a unique fracture tendency: first, after elastic deformation, the composites elongate gradually and display a plateau region at high strain corresponding to plastic deformations; second, the stress/strain derivative ($d\sigma/d\varepsilon$) increases as the composites stretch, especially at the latter part of the stress–strain curve, indicating the material becomes more robust when larger stress is applied.

3.2.2 Effect of CNT length. To compare the effects of CNT length, w-CNTs (treated with H_2O_2–H_2SO_4 solution) and s-CNTs (cut by mixed H_2SO_4–HNO_3 solution) were employed as control samples. Fig. S3† shows the w-CNTs were rarely reduced

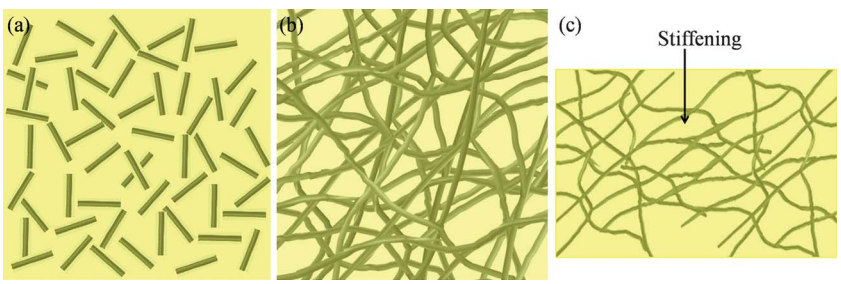

Fig. 4 (a) Random short CNT reinforced nanocomposite. (b) Long-CNT-induced three-dimensional crosslinking network as effective scaffold for load transfer. (c) The CNT network tends to be stiffened under deformation.

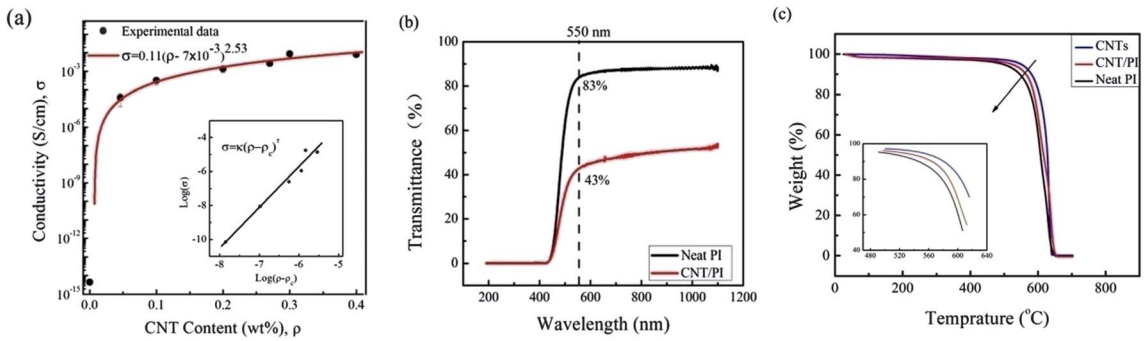

Fig. 5 (a) The variation of volume conductivity with long CNT content, insert is the log-log curve. (b) UV-vis light transmittance curves of neat PI and CNT/PI nanocomposite with a thickness of 23 μm. (c) TGA traces of neat PI and CNT/PI composite films.

and maintained a length distribution in the range of 10–18 μm. In contrast, the conventional oxidizing route using strong acid mixture cut the nanotubes into pieces with a length distribution of 0.8–2.4 μm. Both CNTs were incorporated into PI with good dispersion at 0.27 wt% content (Fig. S4†). Similar surface functional groups were observed on FTIR spectra (Fig. S5†). The different improvement behaviors of mechanical properties are attributed to CNT length. When w-CNTs were used, a similar stress–strain curve to that of CNT/PI was observed (Fig. 2c). The tensile strength of w-CNT/PI is 146.0 MPa at 130% strain, which results in a toughness of 106.8 kJ kg^{-1}. When using short s-CNTs, the s-CNT/PI composite only has an improved tensile strength of 106.6 MPa at a strain of 109% compared to pure PI. The plateau region of s-CNT/PI corresponding to plastic deformation is highly compromised, thus the toughness is reduced to 69.2 kJ kg^{-1}, compared to CNT/PI and w-CNT/PI nanocomposites. Because CNT carboxylation by H_2SO_4–HNO_3 solution degrades the graphitic structure and shortens the length, composites made from s-CNTs are less tough than those made from long CNTs and w-CNTs. Similar trends were observed in recent studies on CNT/polypropene (PP)[16] and CNT/poly (methyl methacrylate) (PMMA) composites,[17] which supports the effective reinforcement of long CNTs.

3.3 Reinforcement mechanism

Fig. 2d depicts the schematic illustration of the reinforcement mechanism of CNT/PI nanocomposites. Though PI is a stiff polymer, it is still soft compared to rigid CNTs. At low strain (I), the interaction between PI and CNTs is limited due to the low elasticity of polymer coils in the elastic deformation region. As deformation increases, the soft PI molecules stretch to accommodate the deformation (II); therefore, the CNT/PI nanocomposites get stiffer, which improves the load bearing capability in the axial direction. Based on good interfacial bonding with CNTs, the nanocomposite strength improves with increasing deformation. Such a phenomenon is pronounced for long CNTs, which provides a large number of anchoring sites for stress transfer. High deformation was also detected (Fig. 2c). Thus, at high deformation (III), the polymer chains are highly stretched and aligned along the *c*-axis of CNTs. Cooperative deformation of the soft and hard segments resulted in the formation of tapered fibrils (IV), enhancing the composites ductility. Hence, energy is well dissipated because PI matrix mobility and CNT strength are cooperatively involved.

3.3.1 Taper fibril morphology on the cross-sections of CNT/PI nanocomposite. In order to further confirm the reinforcement mechanism, the structure and morphology of the composites after stretching were characterized by electron microscopy. SEM images suggest entire cross-sections of the long-CNT-reinforced PI nanocomposites were rough and many tapered fibrils were visually presented on the fracture edges (Fig. 3a). Tapered fibril structure were 250–600 nm in length, with large roots of 85–145 nm and small tips of 16–24 nm in diameter (Fig. S6†). The different size distributions of roots and tips indicate the original PI layers coated on CNT creep along the axial direction of CNTs during stretching. The fractured w-CNT/PI composites display similar tapered fibril structure to these of CNT/PI films (Fig. S7a†). However, the highly oxidized s-CNT/PI nanocomposites show only some nanotube ends pulled out of the PI matrix and scattered on fracture edges (Fig. S7b†). In contrast, Fig. S8† shows that larger tapered fibrils were developed by ultra-long CNTs with lengths up to several millimeters. There is good wetting at the CNT/PI interface, which ensures that CNTs contribute to the strength and toughness of the composite. Thus, after fracture, most CNTs in the matrix are broken. This is evidenced by the uniformly dispersed bright dots on the tapered tip, corresponding to broken CNTs. Fig. 3b shows the microstructure of the tapered fibrils observed under TEM. There are tapered fibrils with a decreasing shape around the nanotube tips. The tapered fibrils were formed among cracks along CNTs under

Table 1 Comprehensive properties of neat PI and 0.27 wt% CNT/PI composite

Sample	Tensile strength (MPa)	Tensile modulus (MPa)	Elongation at break (%)	Toughness (kJ kg^{-1})	Conductivity (S cm^{-1})	5% Thermal decomposition (°C)
Neat PI	81.9	960.6	42	22.4	4.6×10^{-15}	496
CNT/PI	152	1013.0	150	127.4	2.6×10^{-3}	541

tension. These characterization results support the proposed toughening mechanism proposed in Fig. 2d.

3.3.2 Long-CNT induced effective load transfer. To further understand the toughening mechanism, effective load transfer in the interfacial region was estimated. Using an idealized force balance of the tapered microstructure of CNT/PI nanocomposites, interface shear strength (τ_i), connecting PI and CNTs is obtained as follows:[18]

$$\tau_i = \frac{\sigma \cdot D}{2l_c}\left(1 - \frac{d^2}{D^2}\right) \quad (1)$$

where σ is the strength of the CNTs, D and d are the outer and inner diameters of CNTs, and l_c is the critical length. When eqn (1) is fitted to the data of the measured CNTs and the tapered fibrils, τ_i is estimated to be more than 200 MPa.

The calculated interfacial strength affords the good interfacial bonding that was observed between the CNTs and PI before fracture. On one hand, PI at the CNT/PI interface is well trapped locally, making an interfacial region different from bulk PI. Since the bulk PI macromolecules are soft, their molecular mobility is high. The continuous mobility of both PI and CNTs occurs naturally when an external load is applied. The correlated evolution of such mobility initiates the stiffening of trapped PI, and the formation of heterogeneous fibrils. As a result, CNTs cannot be pulled out of the matrix, but rather tightly packed with PI macromolecules and act as strong stress concentrators.

It should be noted that tapered fibrils are unique to long CNT/PI nanocomposites. In-depth reasons are proposed and shown in Fig. 4. As evidenced, when CNTs such as s-CNTs are used as fillers, they are distributed randomly in the PI matrix (Fig. 4a). Compared to CNTs, the bulk polymer is weak. Scissors effect easily creates cracks of composites. Thus, the improvement is not fully exploited due to the premature rupture of composites. In contrast, a CNT network in a matrix can be formed by very long CNTs. The trapped polymers along CNTs transform into a three-dimensional continuous network in the PI matrix (Fig. 4b), which can effectively dissipate load. Thus, long CNTs initiate a long-range creep, which produces the tapered fibrils. They are robust to withstand high deformation, and stiffen the PI chains to increase the composite strength. Thus, a self-reinforcement mechanism occurs to toughen nanocomposites (Fig. 4c). The high deformation naturally produces tapered fibrils in the long CNT reinforced nanocomposites.

3.4 Multi-functional properties of CNT/PI nanocomposite

To fully demonstrate the multifunctional applications of the nanocomposites, the electrical, optical, and thermal properties of the as-prepared CNT/PI films were also tested.

As shown in Fig. 5a, the conductivity of pure PI is 4.6×10^{-15} S cm^{-1}. The conductivity of PI nanocomposites increases dramatically to 3.8×10^{-5} S cm^{-1} with 0.046 wt% CNT addition. When the CNT content further increases to 0.27 wt%, the electrical conductivity increases to 2.6×10^{-3} S cm^{-1}, which is over 10 orders of magnitude higher than that of neat PI (Table 1). By fitting the data according to percolation theory, the percolation threshold of the nanocomposite is 0.007 wt%, which is among the smallest values ever reported for CNT/PI composites.[12,19] Herein, the long CNTs were well dispersed in the PI matrix. The low percolation threshold is attributed to the web-like conductive networks easily formed by long CNTs.

The UV-vis spectra of 23 μm thick films are illustrated in Fig. 5b. The CNT/PI nanocomposites are uviofast with a light threshold at 436 nm to cut off all UV irradiation. Since the CNT content of the nanocomposite is very low (0.27 wt%), the as-obtained CNT/PI films are optically transparent. For the reason that CNTs in nanocomposites enhance light absorption, scattering and reflection, a loss of transmittance was observed. However, the transmittance of 0.27 wt% CNT/PI film still maintains up to 43% at 550 nm. Here, we should note that the thickness of the tested composite is 23 μm, which is hundreds of times greater than that of typical reported transparent conductive films. By reducing film thickness, their transparency is expected to be improved. Hence, uviofast window coatings in buildings are a feasible application of such CNT/PI nanocomposites.

Thermal stability is important when considering high temperature applications of the nanocomposites. TGA was conducted in air flow and the results are shown in Fig. 5c. CNT addition increases the thermal stability of PI films. Pure PI films begin to decompose (>5% weight loss) at 496 °C and 50% weight loss occurs at 584 °C. However, the addition of 0.27 wt% CNTs slows the decomposition temperature to 541 °C with 50% weight loss at 617 °C. The enhanced thermal stability is because PI chains near the isolated nanotube surfaces are less mobile.[20] Besides, the diffusion of the degradation products is hindered due to the CNT addition. These nanocomposites could withstand tough high temperature applications.

4. Conclusions

In summary, we have demonstrated dramatic improvements in the toughness of CNT/PI nanocomposites by a long-CNT-induced long-range creep, which brings on a self-reinforcing mechanism. Robust tapered fibrils form around high-aspect-ratio CNTs and enhance their capability to absorb energy during deformation. Such a tapered fibril structure is more effective for energy dissipation compared to CNT debonding and low deformation breakage mechanism. Consequently, the composites with a small amount of nanotubes (0.27 wt%) exhibit high toughness up to 127.4 J g^{-1}, which is a 4.7-times improvement compared to pure PI. The long CNTs embedded in the PI matrix construct a conducting network simultaneously, and impart an ultra-low electron-percolation threshold of 0.007 wt% to the nanocomposites. Moreover, the as-prepared CNT/PI films possess high thermal stability and transparency. Thus, such nanocomposites could find various applications as advanced structural and functional materials.

Acknowledgements

The work was supported by the Foundation for the Natural Scientific Foundation of China (No. 20736007, No. 2007AA03Z346), and the China National Program (No. 2011CB932602). The authors thank Peng Li for the helpful discussion.

References

1 M. E. Launey and R. O. Ritchie, *Adv. Mater.*, 2009, **21**, 2103; N. Du, Z. Yang, X. Y. Liu, Y. Li and H. Y. Xu, *Adv. Funct. Mater.*, 2011, **21**, 772; U. Khan, P. May, A. O'Neill, J. J. Vilatela, A. H. Windle and J. N. Coleman, *Small*, 2011, **7**, 1579.

2 M. T. Byrne and Y. K. Gun'ko, *Adv. Mater.*, 2010, **22**, 1672; J. N. Coleman, U. Khan, W. J. Blau and Y. K. Gun'ko, *Carbon*, 2006, **44**, 1624; P. M. Ajayan and J. M. Tour, *Nature*, 2007, **447**, 1066.

3 H. Qian, E. S. Greenhalgh, M. S. P. Shaffer and A. Bismarck, *J. Mater. Chem.*, 2010, **20**, 4751.

4 P. M. Ajayan, O. Stephan, C. Colliex and D. Trauth, *Science*, 1994, **265**, 1212; A. B. Dalton, S. Collins, E. Munoz, J. M. Razal, V. H. Ebron, J. P. Ferraris, J. N. Coleman, B. G. Kim and R. H. Baughman, *Nature*, 2003, **423**, 703; Q. F. Cheng, J. W. Bao, J. Park, Z. Y. Liang, C. Zhang and B. Wang, *Adv. Funct. Mater.*, 2009, **19**, 3219; Q. F. Cheng, B. Wang, C. Zhang and Z. Y. Liang, *Small*, 2010, **6**, 763; L. C. Tang, H. Zhang, X. P. Wu and Z. Zhang, *Polymer*, 2011, **52**, 2070.

5 J. N. Coleman, U. Khan and Y. K. Gun'ko, *Adv. Mater.*, 2006, **18**, 689.

6 Y. C. Jung, D. Shimamoto, H. Muramatsu, Y. A. Kim, T. Hayashi, M. Terrones and M. Endo, *Adv. Mater.*, 2008, **20**, 4509.

7 F. Wei, Q. Zhang, W. Z. Qian, H. Yu, Y. Wang, G. H. Luo, G. H. Xu and D. Z. Wang, *Powder Technol.*, 2008, **183**, 10; Q. Zhang, J. Q. Huang, M. Q. Zhao, W. Z. Qian and F. Wei, *ChemSusChem*, 2011, **4**, 864.

8 K. J. Ziegler, Z. N. Gu, H. Q. Peng, E. L. Flor, R. H. Hauge and R. E. Smalley, *J. Am. Chem. Soc.*, 2005, **127**, 1541; N. Grossiord, J. Loos, O. Regev and C. E. Koning, *Chem. Mater.*, 2006, **18**, 1089; S. Y. Fu, Z. K. Chen, S. Hong and C. C. Han, *Carbon*, 2009, **47**, 3192.

9 N. Grossiord, J. Loos, L. van Laake, M. Maugey, C. Zakri, C. E. Koning and A. J. Hart, *Adv. Funct. Mater.*, 2008, **18**, 3226.

10 L. W. Qu, Y. Lin, D. E. Hill, B. Zhou, W. Wang, X. F. Sun, A. Kitaygorodskiy, M. Suarez, J. W. Connell, L. F. Allard and Y. P. Sun, *Macromolecules*, 2004, **37**, 6055.

11 W. J. Chou, C. C. Wang and C. Y. Chen, *Compos. Sci. Technol.*, 2008, **68**, 2208; C. Park, R. E. Crooks, E. J. Siochi, J. S. Harrison, N. Evans and E. Kenik, *Nanotechnology*, 2003, **14**, L11; Q. H. Zhang, J. Li, X. Zhao and D. J. Chen, *Polym. Int.*, 2009, **58**, 557; M. Lebron-Colon, M. A. Meador, J. R. Gaier, F. Sola, D. A. Scheiman and L. S. McCorkle, *ACS Appl. Mater. Interfaces*, 2010, **2**, 669; Q. Y. Tang, Y. C. Chan, N. B. Wong and R. Cheung, *Polym. Int.*, 2010, **59**, 1240; Q. Y. Tang, J. Chen, Y. C. Chan and C. Y. Chung, *Polym. Degrad. Stab.*, 2010, **95**, 1672; J. L. Tsai, S. H. Tzeng and Y. T. Chiu, *Composites, Part B*, 2010, **41**, 106; F. C. Yang, Y. F. Li, S. J. Zhang, M. Tao, J. J. Zhao and C. S. Hang, *Synth. Met.*, 2010, **160**, 1805; M. Q. Zhao, Q. Zhang, X. L. Jia, J. Q. Huang, Y. H. Zhang and F. Wei, *Adv. Funct. Mater.*, 2010, **20**, 677; M. A. Aroon, A. F. Ismail, M. M. Montazer-Rahmati and T. Matsuura, *J. Membr. Sci.*, 2010, **364**, 309; C. Fang, J. N. Zhao, J. J. Jia, Z. G. Zhang, X. H. Zhang and Q. W. Li, *Appl. Phys. Lett.*, 2010, **97**, 181906.

12 D. C. Wu, L. Shen, J. E. Low, S. Y. Wong, X. Li, W. C. Tjiu, Y. Liu and C. Bin He, *Polymer*, 2010, **51**, 2155.

13 Q. Zhang, M. Q. Zhao, Y. Liu, A. Y. Cao, W. Z. Qian, Y. F. Lu and F. Wei, *Adv. Mater.*, 2009, **21**, 2876; Q. Zhang, M. Q. Zhao, J. Q. Huang, J. Q. Nie and F. Wei, *Carbon*, 2010, **48**, 1196.

14 G. H. Xu, Q. Zhang, J. Q. Huang, M. Q. Zhao, W. P. Zhou and F. Wei, *Langmuir*, 2010, **26**, 2798.

15 J. N. Coleman, M. Cadek, R. Blake, V. Nicolosi, K. P. Ryan, C. Belton, A. Fonseca, J. B. Nagy, Y. K. Gun'ko and W. J. Blau, *Adv. Funct. Mater.*, 2004, **14**, 791; C. Han Gi and S. Kumar, *J. Appl. Polym. Sci.*, 2006, **100**, 791; I. O'Connor, H. Hayden, J. N. Coleman and Y. K. Gun'ko, *Small*, 2009, **5**, 466.

16 J. L. Yang, Z. Zhang, K. Friedrich and A. K. Schlarb, *Macromol. Rapid Commun.*, 2007, **28**, 955.

17 X. M. Sui and H. D. Wagner, *Nano Lett.*, 2009, **9**, 1423.

18 H. D. Wagner, O. Lourie, Y. Feldman and R. Tenne, *Appl. Phys. Lett.*, 1998, **72**, 188.

19 Z. Spitalsky, D. Tasis, K. Papagelis and C. Galiotis, *Prog. Polym. Sci.*, 2011, **35**, 357; C. A. Martin, J. K. W. Sandler, M. S. P. Shaffer, M. K. Schwarz, W. Bauhofer, K. Schulte and A. H. Windle, *Compos. Sci. Technol.*, 2004, **64**, 2309; X. W. Jiang, Y. Z. Bin and M. Matsuo, *Polymer*, 2005, **46**, 7418; D. Thuau, V. Koutsos and R. Cheung, *J. Vac. Sci. Technol., B: Microelectron. Nanometer Struct.–Process., Meas., Phenom.*, 2009, **27**, 3139.

20 W. Zhang, I. Srivastava, Y. F. Zhu, C. R. Picu and N. A. Koratkar, *Small*, 2009, **5**, 1403.

